ACS APPLIED MATERIALS & INTERFACES

Research Article

www.acsami.org

Three-Dimensional Rapid Prototyping of Multidirectional Polymer Nanoprobes for Single Cell Insertion

Dasom Yang, Hyeonaug Hong, Yoon Ho Seo, Lo Hyun Kim, and WonHyoung Ryu*

Department of Mechanical Engineering, Yonsei University, 50 Yonsei-ro, Seodaemun-gu, Seoul 120-749, Republic of Korea

Supporting Information

ABSTRACT: Three-dimensional (3D) thermal drawing at nanoscale as a novel rapid prototyping method was demonstrated to create multidirectional polymer nanoprobes for single cell analysis. This 3D drawing enables simple and rapid fabrication of polymeric nanostructures with high aspect ratio. The effect of thermal drawing parameters, such as drawing speeds, dipping depths, and contact duration on the final geometry of polymer nanostructures was investigated. Vertically aligned and L-shaped nanoprobes were fabricated and their insertion into living single cells such as algal cells and human neural stem cells was demonstrated. This technique can be extended to create more complex 3D structures by controlling drawing steps and directions on any surface.

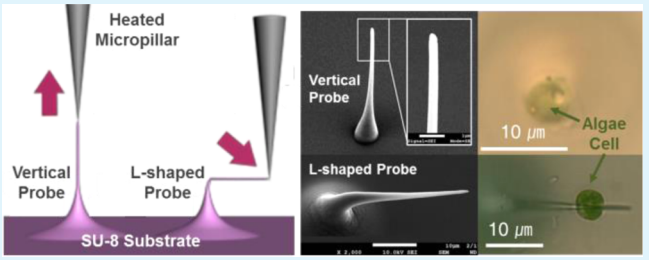

KEYWORDS: *3D thermal drawing, multidirectional, nanoprobes, cell insertion, rapid prototyping*

INTRODUCTION

Understanding biological events at a subcellular level requires analytical tools to be brought into the cell interior. Recent efforts to monitor biological signals at a single cell or smaller resolutions employed nanowire[1−6] or nanoneedle structures[7−10] to directly sense or to interfere molecular interactions. However, these nanowire-type sensors were limited in detecting biomolecular interactions on the membrane surface or in the vicinity of target cells.[2,4,5] For accurate understanding of biological phenomena in cell interior, it is desired to bring probing tools into the cytosol space.[11,12] Although various fabrication technologies for such cell-probing tools such as nanowires have been developed, it is still challenging and expensive to fabricate sufficiently small and tall nanowires for minimally invasive analysis. In this study, we present a rapid prototyping technique of fabricating polymeric nanowires as cell-probing nanostructures using thermal drawing of thermoplastic materials. This technique allows for rapid and low-cost fabrication of individual and customized-control of nanowire-type probes suitable for cell probing.

Previously, drawing-based approaches for nanowire fabrication have been demonstrated using AFM probes or micropipettes. The approach using AFM probe used either dilute or semidilute polymer solutions for fiber drawing and relied on solvent evaporation for the final solidification of the drawn polymer shapes.[13,14] However, maintaining uniform viscosity during drawing processes is extremely difficult due to solvent evaporation. This hinders controlled and uniform fabrication of polymer nanostructures in a serial process. On the other hand, direct writing by micropipette has also been developed for 3D metal or conducting polymer nanowires. Metallic nanowires were fabricated by depositing an electrolyte ink through a nanoscale meniscus under an electric field.[15] By taking a similar approach, we shaped conducting polymer as 3D nanowires based on meniscus-guided polymerization.[16] However, these approaches require rather a complex setup and are applicable to limited conditions and materials. For example, such electrochemically deposited metallic nanowires can be formed only on a metallic surface. Meniscus-guided writing of conducting polymer is possible only with materials that can be polymerized by oxygen.

Here, we present "three-dimensional (3D) thermal drawing" as a versatile rapid prototyping method at nano scale. This method offers precision fabrication of nanowire structures like the above techniques. However, the simplicity and reversibility of this approach gives clear distinction from other alternative solutions. This 3D thermal drawing can be applied to any thermoplastic materials giving much broader selection of materials to use. Use of local heating can easily create and remove nano features reversibly. Such reversibility of the approach enables convenient modification, addition, and removal of the previously fabricated polymer nanostructures. Using this thermal drawing, high aspect-ratio nanowires were fabricated to demonstrate their insertion capability into single cells, which is required as cell-probing structures.

EXPERIMENTAL SECTION

Materials. SU-8 2150 was purchased from Microchem and Rhodamine B (product no. R0050, RB) was purchased from Samchun Chemical. Tungsten nanopillar (product no. 13570-10) in 600 nm diameter was purchased from Ted Pella Inc. The green alga *Chlamydomonas reinhardtii* (CC-4348, cell wall-less strain, Chlamydo-

Received: June 15, 2015
Accepted: July 6, 2015
Published: July 6, 2015

DOI: 10.1021/acsami.5b05254
ACS Appl. Mater. Interfaces 2015, 7, 16873−16880

Scheme 1. (a) Schematic Diagram of Vertically-Aligned Polymer Nanowires Using Thermal Drawing and (b) Fabrication Steps of Multi-Directional Polymer Nanowires

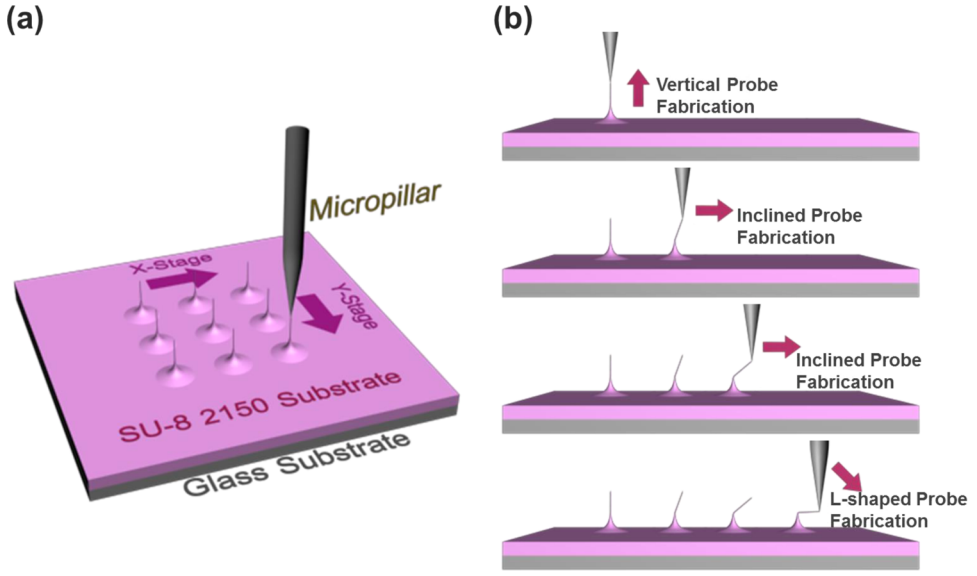

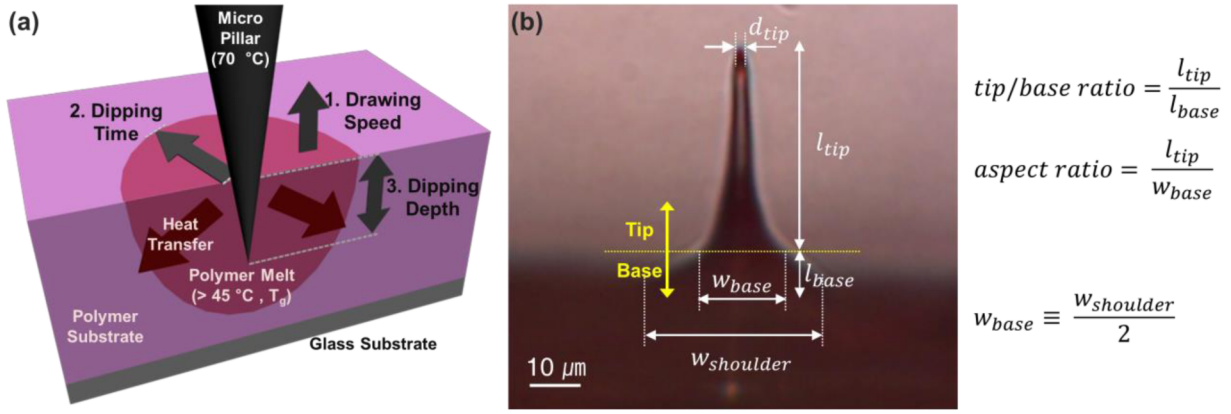

Figure 1. (a) Schematic diagrams of the effect of drawing speed, dipping duration and dipping depth on the amount of polymer melt. (b) Drawing parameters of thermally drawn polymer nanostructure.

monas Resource Center) was cultured tris−acetate−phosphate (TAP) medium which was prepared by mixing 2.42 g of Tris base, 25 mL of TAP salts solution, 1.0 mL of phophate solution, 1.0 mL of Hunter trace elements, 1.0 mL acetic acid and deionized water to 1 L. Human nueral stem cells (hNSCs) was prepared with N-2 Supplement (N2) and penicillin-streptomycin (PS) added Dulbecco's modified Eagle's medium (DMEM)/F12 medium. Around 10 μm sized cells were used in cell insertion experiment.

Thermal Drawing System. A tungsten micropillar was connected to a micro heater (NEWINS Inc.) that was fixed in a stand. Thermocouples (catalog no. 5TC-GG-K-3636, Omega Engineering Inc.) were attached to the micropillar and a polymer substrate. Their temperatures were separately monitored and controlled using a temperature controller. A custom-built thermal drawing stage was manipulated in x and y directions at a micrometer scale. A z-direction movement was automatically controlled using a step motor.

Nanoprobe Fabrication. SU-8 2150 was spin coated on a glass or silicon substrate and soft baked for solvent removal. Since Tg of SU-8 2150 is 45 °C, a tungsten micropillar heated at 70 °C and the temperature of SU-8 substrate was maintained at 40 °C. After the micropillar and polymer substrate were heated to their desired temperatures, the polymer substrate was gradually lifted until the micropillar was dipped to a desired depth. After predetermined contact duration, the polymer substrate was lowered down at a predetermined speed until the liquid bridge of the drawn polymer structure broke by surface tension.

Nanoprobe Insertion into Cells. An array of polymer nanoprobes with 450 nm tip ends was prepared. TAP medium containing Chlamy cells (5.291×10^5 cells/ml) and N2, PS added DMEM/F12 medium containing hNSCs (500 cells/ml) were prepared. Using a micropipette of our custom-built single cell analysis system, a single cell was captured and held at the tip of the micropipette by vacuum. The captured single cell was moved above a target polymer nanoprobe by a 3D micromanipulator. The cell was gently moved and the nanoprobe was inserted without any rupture of cell membranes. Afterward, the cell was released from the micropipette when the insertion was complete.

RESULTS AND DISCUSSION

Scheme 1a shows a schematic diagram of the 3D thermal drawing method. First, a heated metallic micropillar makes a contact on a target location of a polymer layer and heats locally to give enough thermal mobility to polymer chains in the vicinity. Then, the nanoprobe is lifted and starts drawing the polymer to form a vertical nanowire shape. After forming a neck-shaped liquid bridge, the drawn polymer is further pulled upward until the neck breaks off. When we move the pillar in the x direction before the neck breaks off, the drawn polymer is inclined along the pillar

DOI: 10.1021/acsami.5b05254
ACS Appl. Mater. Interfaces 2015, 7, 16873−16880

from the contact point. If pillar moves further, polymer wire become more inclined and finally forms an L-shape wire (Scheme 1b). In particular, there are several parameters that mainly affect the thermally drawn nanostructures, such as drawing temperature (substrate and pillar), drawing speed, dipping depth and duration (Figure 1a).

First, in thermal drawing, temperature is a key parameter that determines the mobility of polymer chains and the viscosity of heated polymer. Higher temperature in general increases polymer mobility and allows for drawing of polymer in thin fiber forms. However, too high temperature can cause premature breakup in the drawn polymer before drawing completes. Once drawing to a desired height is complete, separation of the drawn polymer from the metal pillar is required to form a tip at the end of the drawn polymer structure. Fast drawing at low temperature for tip formation causes the uncontrolled bending or elongation of polymer structures due to the residual stress after fracture at the neck. On the other hand, at high pillar temperatures, the amount of mobile polymer chains increases and it becomes much easier to form sharp tips after breakup at the neck of drawn polymer structures. In this study, since the glass transition temperature (T_g) of unexposed SU-8 2150 is around 50 °C, substrate temperature was fixed at 40 °C just below T_g to prevent undesired deformation after drawing and the pillar temperature was set at 70 °C. During thermal drawing, as a distance between pillar and substrate increases after drawing, predrawn polymer structure cools below T_g by ambient air such that it hardens.

To determine the effect of drawing parameters on the geometry of polymer structures, we defined geometric parameters such as tip diameter (d_{tip}), tip length (l_{tip}), base width (w_{base}), base length (l_{base}), and shoulder width ($w_{shoulder}$) (Figure 1b). The tip/base boundary was defined where the width became the half of the shoulder width. Effect of drawing parameters on geometric factors such as tip/base ratio (l_{tip} /l_{base}), aspect ratio (l_{tip} /w_{base}), base width, and tip diameter were analyzed using the optical silhouettes and SEM images of polymer nanoprobes.

Drawing speed significantly influences the final shape of polymer nanoprobes (Figure 2). As a tungsten pillar moves upward from a polymer substrate, polymer chains that have mobility high enough to flow begin to move following the travel path of the pillar. At this moment, gravity, viscosity, inertial force, and capillary forces caused by surface energy contribute to form the final shape of the drawn polymer structures.[17] Geometric change of the nanoprobes for different drawing speeds can be classified into three different modes: Mode I, slow; Mode II, normal; and Mode III, fast drawing.

As heat moves from a metal pillar to a polymer substrate, polymer chains in the vicinity of the metal pillar have the highest temperature and the lowest shear viscosity. For a fixed height of total drawing, slow drawing leads to longer drawing time and mobilizes more polymer chains. Such slow drawing in the Mode I results in capillary self-thinning and the diameter of drawn polymer necks decreases over time. The self-thinning eventually leads to the premature failure of polymer drawing due to capillary breakup[18] (Figure 2a). In this capillary-thinning mode, increase of drawing speed delayed the point of breakage and resulted in the noticeable increase of aspect ratio (A/R), tip/base ratio, and tip diameter (Figures 2 and 3).

When the drawing became faster (Mode II), normal drawing was observed without premature failure due to capillary-thinning (Figure 2b,c). In this normal drawing mode, as the metal pillar moves away from the polymer substrate at a speed faster than in the Mode I, polymer chains are less affected by the heated metal pillar. This reduces the mobility of polymer chains such that the capillary-thinning becomes less dominant than in Mode I. In this normal drawing mode, rapid decrease of total drawing time reduced the amount of mobile polymer chains that were to be drawn. As a result, the base width and tip diameter significantly decreased for faster drawing speeds (Figure 3b). This reduced base width and tip diameter in turn increased both the A/R and tip/base ratio for faster drawing.

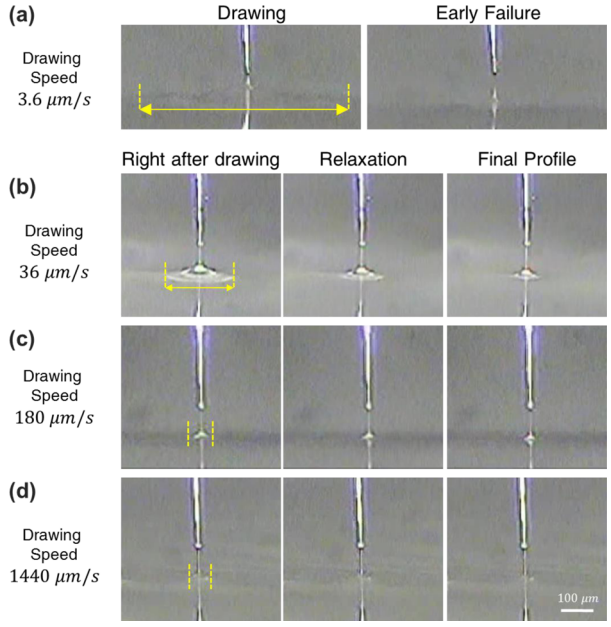

Figure 2. Optical images of thermal drawing process at different drawing speeds of (a) 3.6, (b) 36, (c) 180, (d) 1440 μm/s. Scale bar indicates 100 μm, and yellow lines indicate initial shoulder width in the beginning of drawing. Because drawing height was fixed to 100 μm in all cases, total drawing time was dependent on drawing speed. At slow drawing speed cases, longer process time increased the amount of mobile polymer chains and widened the initial shoulder width of drawn polymer structures.

At even faster drawing speeds (Mode III), both the A/R and tip/base ratios still increased but the increasing trend became smaller (Figures 2d and 3b). At such fast speeds, the metal pillar had much shorter contact time with polymer chains in the polymer substrate. Thus, in the Mode III, the amount of mobile polymer chains that were heated by the metal pillar became limited, and there was no further decrease of the base widths of the drawn polymer structure (the second plot in Figure 3b). This limited reduction of the base width also resulted in the saturation of both the A/R and tip/base ratios (the first plot in Figure 3b). In this fast drawing mode, drawing time was shorter than 0.5 s in all cases such that initial shoulder width was almost constant for drawing speeds. On the other hand, it was also observed that faster drawing lifted more polymer chains due to their large inertial force and ended up increasing tip diameters (the third plot in Figure 3b). This is likely due to the drawing of entangled polymer chains. When polymer chains are pulled at a speed above a certain threshold value, entangled polymer chains are pulled all together (contrary to the reputation motion of polymer chains). Too fast drawing lifts the whole polymer chains altogether instead of inducing reptation-like movement of individual polymer chains.[19] This entangled pulling causes the enlargement of the volume of drawn polymer.

DOI: 10.1021/acsami.5b05254
ACS Appl. Mater. Interfaces 2015, 7, 16873−16880

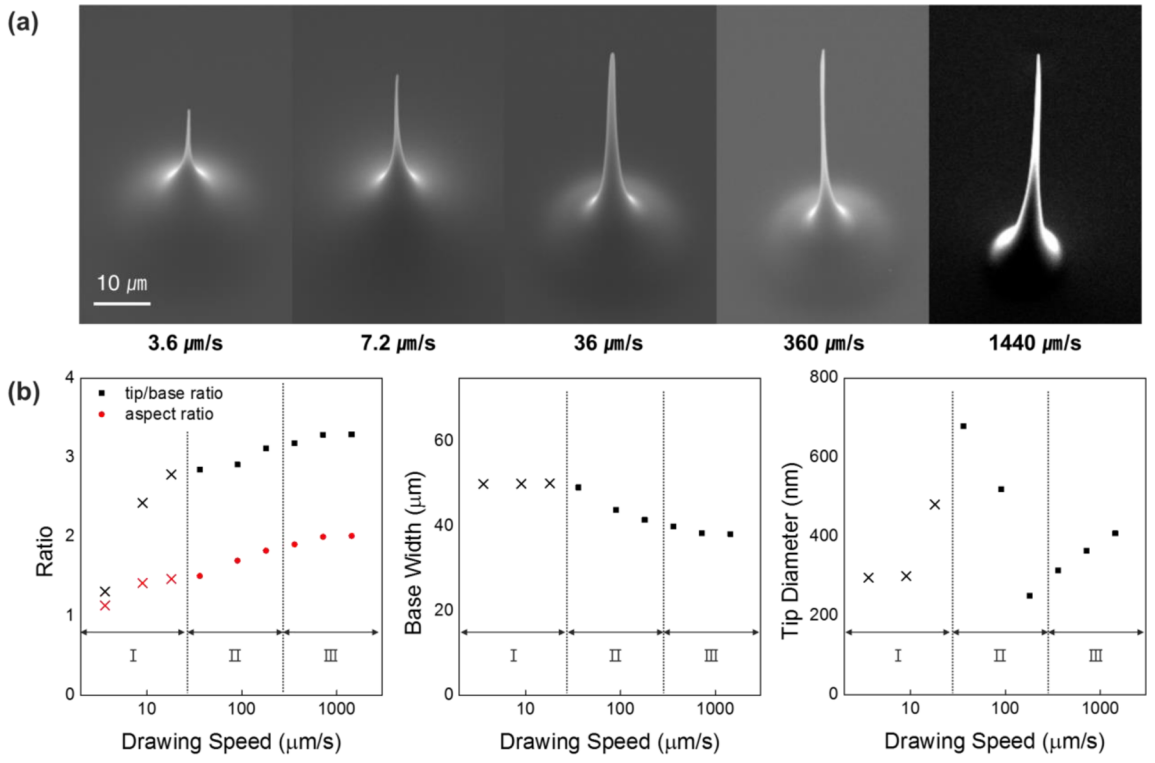

Figure 3. (a) SEM images of thermally drawn polymer nanostructures at different drawing speeds. Dipping duration, depth, and drawing height were fixed at 0 s, 36 μm, and 100 μm, respectively. Tungsten pillars with 0.6 μm tip end diameter were used in all experiment. (b) Plot of aspect ratio, tip-to-base ratio, base width, and tip diameter as a function of drawing speed; × indicates drawing failure. Drawing speed is in log scale.

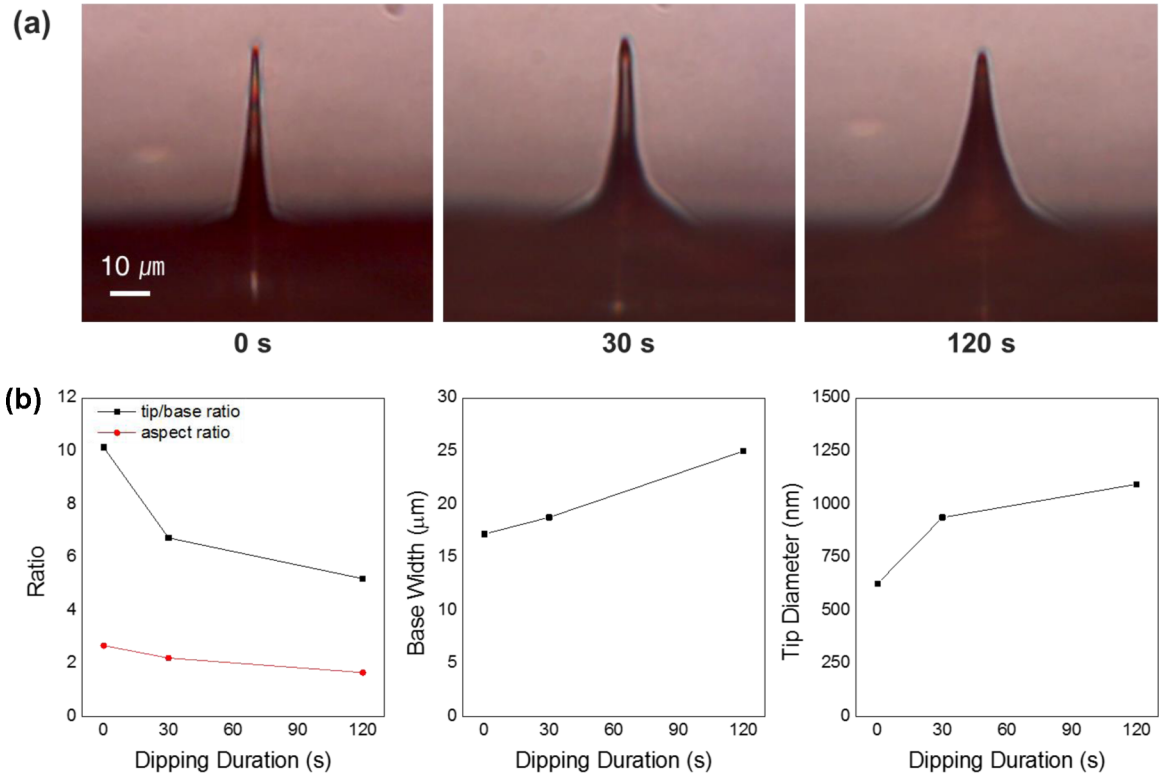

Figure 4. (a) Optical images of polymer nanoprobes with different dipping durations from 0, 30, and 120 s for drawing heights of 54 μm are shown. For all cases, a dipping depth of 36 μm was maintained with drawing speed of 1440 μm/s. (b) Plot of aspect ratio, tip-to-base ratio, base width, and tip diameter as a function of dipping duration.

From this tip diameter−drawing speed study, drawing at a speed of 180 μm/s produced the smallest tip diameter (Figure 3b). However, drawing at this speed often caused uncontrolled bending of nanoprobes due to the stretching and subsequent

DOI: 10.1021/acsami.5b05254
ACS Appl. Mater. Interfaces 2015, 7, 16873−16880

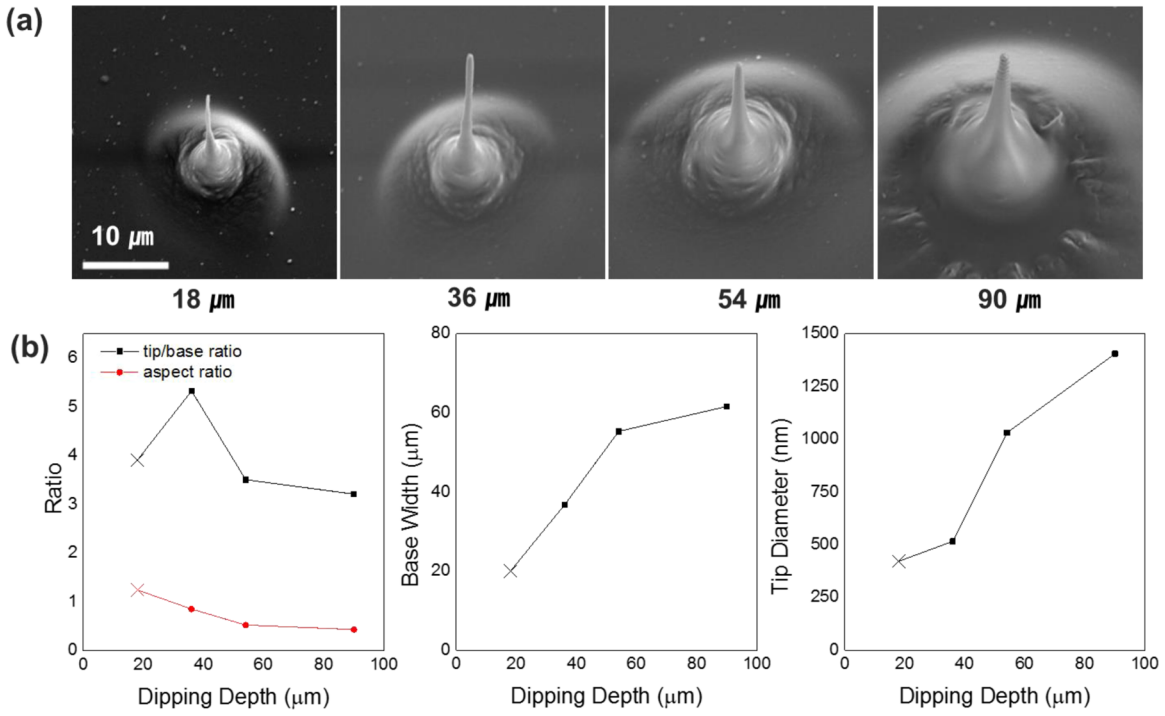

Figure 5. (a) SEM images of polymer nanoprobes fabricated with different dipping depth conditions. Dipping depth was varied from 18, 36, 54, to 90 μm with a drawing speed of 1440 μm/s, drawing height of 54 μm, and instantaneous dipping contact. Scale bar indicates 10 μm. (b) Plot of aspect ratio, tip-base ratio, base width and tip diameter as a function of dipping depth. "x" indicates drawing failure.

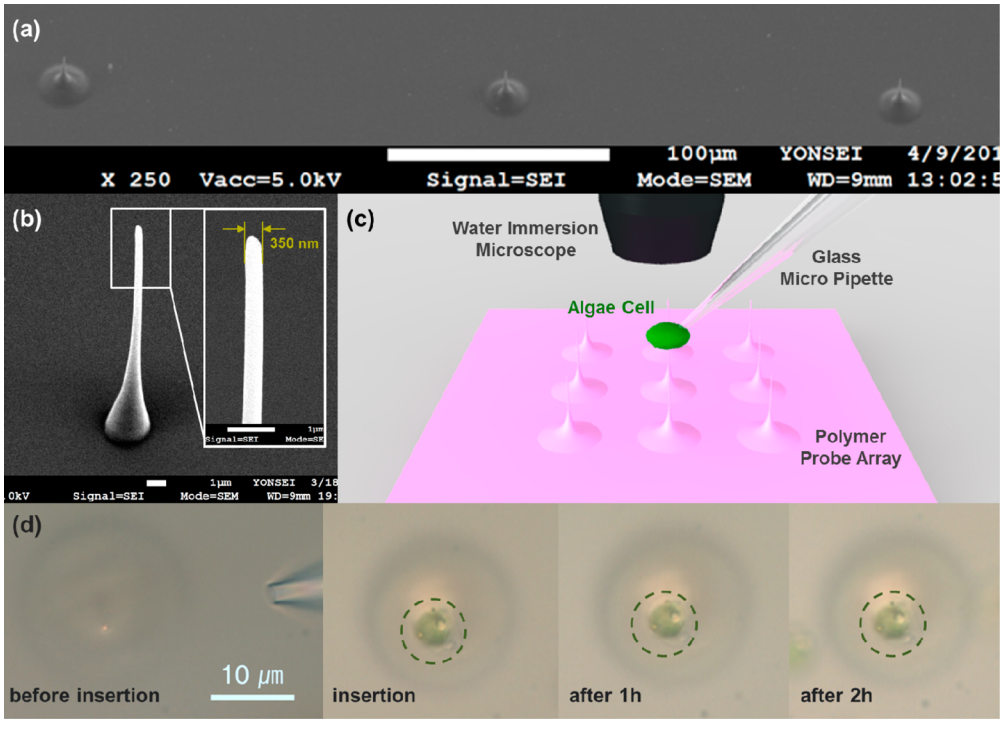

Figure 6. SEM images of (a) an array of thermally drawn nanoprobes with average tip diameter of 450 nm and (b) zoomed-in view of a single nanoprobe with the smallest tip diameter (350 nm). (c) Schematic diagram of single cell analysis system used for nanoprobe insertion. (d) Optical images of cell insertion and time-lapse image of cell morphology after nanoprobe insertion. The green circle indicates the inserted cell.

breakage at the neck of the drawn polymer structure (data not shown).[20] In our experiment, at 1440 μm/s, more repeatable drawing without such stretching or bending at the neck breakage was observed and the drawing speed was used for further experiments.

Dipping duration of the tungsten pillar in a polymer substrate also has a significant influence on thermal drawing process. The dipping duration determines the amount of mobile polymer chains, which affects the viscosity of drawn polymer. Increase of dipping duration induces more heat transfer from the pillar to the

DOI: 10.1021/acsami.5b05254
ACS Appl. Mater. Interfaces 2015, 7, 16873−16880

Table 1. Dimensions of Fabricated Polymer Nanoprobes

length (μm)			width (μm)	diameter (nm)	ratios	
total	tip	base	shoulder	tip	tip/base	aspect
24.378 (±1.294)	16.872 (±0.986)	7.506 (±0.439)	4.186 (±0.506)	452.429 (±24.975)	2.286 (±0.145)	8.839 (±0.898)

*Number of samples =9.

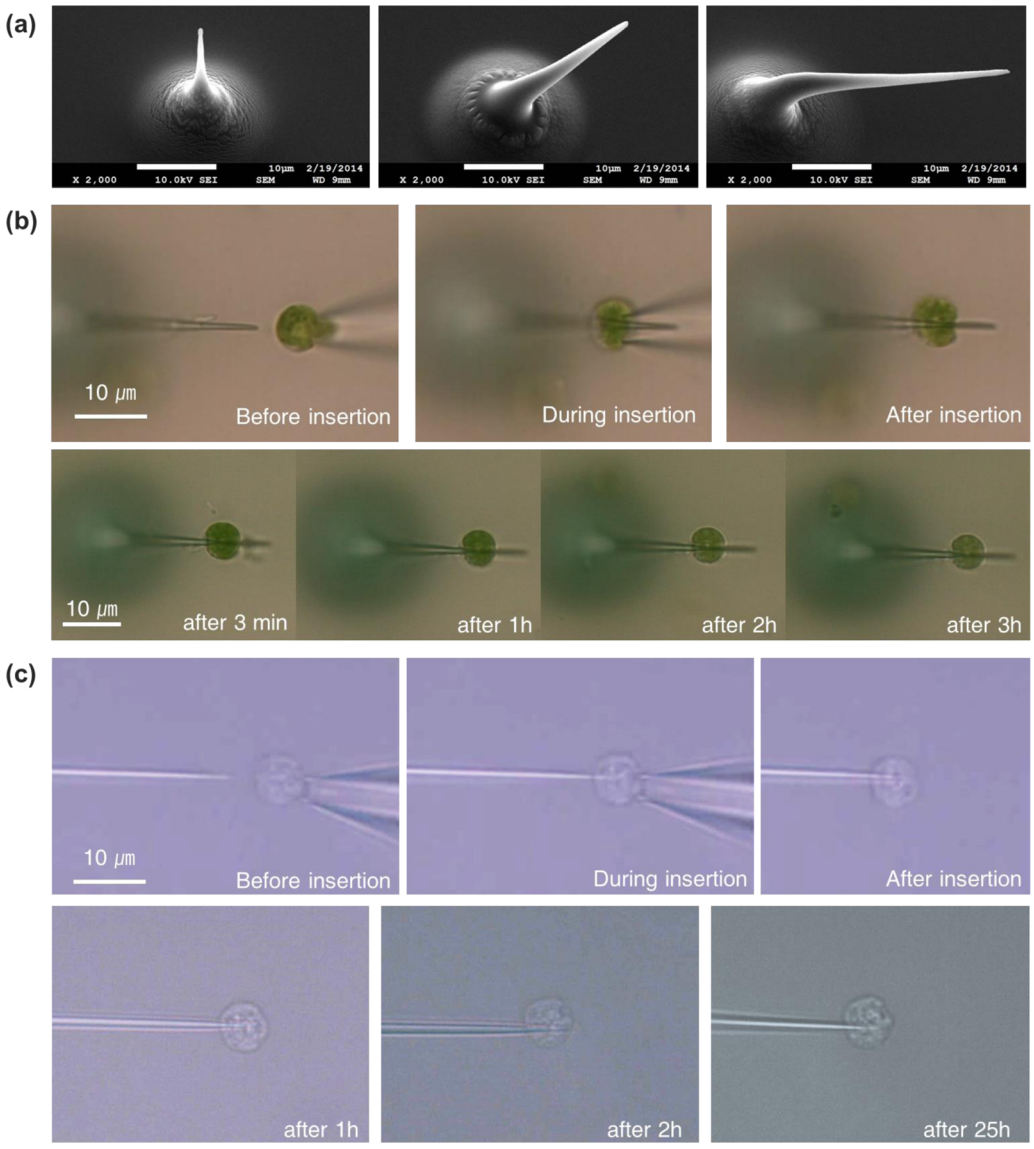

Figure 7. (a) SEM images of vertically aligned, inclined, and L-shaped polymer structure. Optical images of (b) algae cell and (c) human neural stem cell insertion process and time-lapse images with L-shaped polymer structure.

polymer and more polymer chains become mobile (Figure 1a). For all cases, the dipping depth was 36 μm with drawing speed of 1440 μm/s. Drawing height was maintained as 54 μm for all experiments. Figure 4a shows the optical images of polymer nanoprobes for the dipping time of 0 (instant contact), 30, and 120 s. As shown in Figure 4b, when the drawing height was maintained identical for all cases, longer dipping duration tends to produce polymer nanoprobes with wider shoulders and obtuse tip ends. Shorter contact produced much sharper and more slender probe shapes. Thus, in order to fabricate a polymer probe with high aspect ratio and smaller tip ends, almost instantaneous contact of the tungsten pillar to the polymer substrate is ideal.

Dipping depth also affects the amount of mobile polymer chains. Dipping depth is defined as a distance between a pillar end and the surface of a polymer substrate into which the pillar was dipped (Figure 1a). When dipping depth increased, more polymer chains became mobile, and subsequent drawing produced nanoprobes with larger diameter and wider shoulder. In our experiments, dipping depth was varied from 18 to 90 μm with the identical drawing speed of 1440 μm/s, drawing height of 54 μm, and instantaneous dipping contact. As shown in Figure 5a, shallow dipping produced thinner and sharper nanoprobes that are suitable for intracellular probing. When dipping depth increased, bottom side of polymer probe becomes thicker with blunt tips (Figure 5a,b). This indicates that dipping depth needs

DOI: 10.1021/acsami.5b05254
ACS Appl. Mater. Interfaces 2015, 7, 16873−16880

to be as shallow as possible to fabricate thin nanoprobes with high A/R's by thermal drawing. However, when dipping was done at too shallow depth, polymer drawing often became unstable. In our experiments, drawing usually failed when dipping depth was shallower than 18 μm.

In this drawing process, there were two general types of drawing failure. When drawing performed at a speed below a threshold value, long process time and highly mobile polymer chains resulted in relaxation and early failure during drawing (Figure 2a). As another type of failure, when drawing depth was shallower than 18 μm, the amount of mobile polymer chains was insufficient and drawing above a certain height caused premature breakage during the drawing process (Figure 5b). The final height of the resulting polymer nanoprobe was normally far shorter than a desired height with low success rate of less than 30% under these conditions.

For a cell insertion study, an array of polymer nanoprobes with the average tip diameter of 452 ± 24.975 nm and average height of 25 ± 1.294 μm was prepared for cell insertion test (Figure 6a, Table 1). The thinnest nanoprobe had the diameter of 350 nm as shown in Figure 6b. The nanoprobes were fabricated with dipping depth of 25 μm, instant contact and drawing at a drawing speed of 1440 μm/s. Then, a solution of algal cells, *Chlamydomonas reinhardtii* (Chlamy cell), were prepared for the nanoprobe insertion tests. The algal cell was selected as a model cell to investigate the feasibility of the polymer nanoprobes to directly extract photosynthetic electrons from living algal cells, as reported previously.[21] In our custom-built single cell manipulation system, a single Chlamy cell was held by vacuum using a glass micropipette for 3D manipulation (Figure 6c), as described in our previous work.[22] The cell was moved above a target nanoprobe, and it was gently lowered down until the nanoprobe was inserted. The nanoprobe-inserted cell maintained the original round morphology during 2 h without significant leakage or cell shrinkage (Figure 6d). To confirm the stability of cell insertion, torque was applied to the end of cell by a glass micropipette (Supporting Information, S1). This induced only cell rotation without any breakaway of the cell from the nanoprobe and confirmed the insertion of the nanoprobe into the cell.

In the above fabrication processes, "vertically-aligned" polymeric nanoprobes were fabricated by one-dimensional (1D) movement of a drawing pillar. This approach can be extended to fabricate 3D polymer nanostructures. In particular, the drawing angle was varied from vertical to horizontal directions, multidirectional probes like "inclined" or "L-shaped" nanoprobes were fabricated as a result (Figure 7a). The L-shaped nanoprobe was inserted into a single Chlamy cell using a glass micropipette connected to a micromanipulator (Figure 7b, Supporting Information, S2). The algal cell remained stable after nanoprobe insertion and there was no indication of leakage or membrane deformation. Considering that the algal cell was a mutant strain whose cell wall was removed, it is noteworthy that the nanoprobe penetration did not disrupt the integrity of the cell wall-deficient Chlamy cell. To observe the applicability of the polymer nanoprobe to animal cells, we held a single human neural stem cell (hNSCs) using a glass micropipette and gently inserted the L-shaped nanoprobe into the hNSC (Figure 7c). During insertion, no visible rupture or damage to the cell membrane was found (Supporting Information, S3). Time-lapse images also confirmed the long-term stability of the hNSC after nanoprobe insertion.

This L-shaped polymer probe has a more favorable structure than the vertical probe for cell insertion process. First, the top part of the L-shaped probe was easier to observe than the previous vertical nanoprobe with an optical system. In addition, due to the difference in focal planes, an algal cell and probe cannot be clearly focused at the same time in the vertical probing system. However, the L-shaped probing system does not only allow the simultaneous monitoring of an algae cell but also enables clear and focused vision of cell insertion and bending of polymer probe (Figure 7b,c). Moreover, direction of repulsive force from the polymer probe which occurs during the nanoprobe insertion process may cause disengagement of an algae cell from the holding micropipette in the vertical probing system (Figure 8a). In contrast, in the L-type probing system,

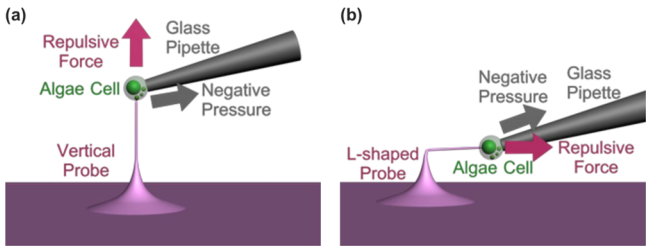

Figure 8. Brief free-body diagram of the cell insertion process with (a) vertical and (b) L-shaped polymer probes.

repulsive force pushes the cell toward the pipet and rather strengthens the holding between cell and pipet (Figure 8b). In general, the L-type probing system showed greatly improved success rate (~50%) than vertical-type probing system (~2%).

In this study, thermal drawing generated nanowire-shaped polymer structures that had the tip diameter in the range between 300 nm and 1 μm. For single cell insertion studies by other groups,[4,5,10] inorganic nanoprobes such as Si or ZnO nanowires with the tip diameter between 200−700 nm have been used for their insertion into animal cells. For algal cells and stem cells in our study, nanoprobes with the diameters of as small as 450 nm were inserted into single Chlamy cells and neural stem cells without immediate breakage of the cell morphology. Although the nanoprobes fabricated by thermal drawing in this study were larger than the state-of-the-art inorganic nanowires, further size reduction of thermally drawn nanoprobes is possible by minimizing the amount of mobile polymer chains. Use of a smaller metal pillar, instantaneous contact on a polymer substrate, shallow dipping, and short drawing distance in thermal drawing processes can generate thinner polymer nanoprobes.

Advantage of thermally drawn nanoprobes over inorganic nanowires is the convenient change of nanowire lengths and directions. In this study, we fabricated nanoprobes with the lengths up to 100 μm within a few seconds. This is much faster than other fabrication techniques such as VLSI or DRIE. Instant change of drawing direction can create nanowire structures with various angles and shapes. This multidirectional nanowire structures can hardly be achieved with the current state-of-the-art bottom-up or top-down nanofabrication technologies by which only slight change of nanowire direction is possible.[23,24]

CONCLUSION

In summary, we have developed a rapid nanoscale prototyping technique based on 3D thermal drawing to fabricate multidirectional nanoscale probes with high A/R for intracellular probing. Nanoprobe shape was dependent on the temperatures of a

DOI: 10.1021/acsami.5b05254
ACS Appl. Mater. Interfaces 2015, 7, 16873−16880

polymer substrate and metal pillar, drawing speed, contact duration, and dipping depth. The effects of such parameters were analyzed and the most optimal parameters to create high A/R nanoprobes with the smallest tip diameters were determined. To demonstrate the performance of thermally drawn nanoprobes, we prepared a model algal cell and neural stem cell, and the insertion of the nanoprobes into the subcellular compartments of the cells was conducted using a custom-developed single cell analysis system. A leak-free insertion was confirmed by time-lapse monitoring of cell morphology. This nanoscale thermal drawing also enables simple and reliable construction of 3D multidirectional nanoscale probes that are more suitable for cell insertion. As a new way to create nanostructures with high A/R, this 3D multidirectional thermal drawing can be utilized as a novel rapid prototyping technique at nanoscale.

■ ASSOCIATED CONTENT

Supporting Information

Video images of an algae cell insertion process with vertically aligned nanoprobe and L-shaped nanoprobe (Video S1, S2) and video images of human neural stem cell insertion process with L-shape nanoprobe (Video S3). The Supporting Information is available free of charge on the ACS Publications website at DOI: 10.1021/acsami.5b05254.

■ AUTHOR INFORMATION

Corresponding Author

*E-mail: whryu@yonsei.ac.kr Phone: +82-2-2123-5821.

Notes

The authors declare no competing financial interest.

■ ACKNOWLEDGMENTS

This work was supported by the National Research Foundation (NRF) of Korea grants funded by the Korea government (MEST No. 2013R1A1A2008360 and MSIP No. 2011-0020285). This work was also supported by the Center for Advanced Meta-Materials (CAMM) funded by the Ministry of Science, ICT and Future Planning as Global Frontier Project (CAMM-2014M3A6B3063716). We would like to thank Prof. Jae-Chul Pyun at Yonsei University for providing algal cells. We also thank Prof. Seung Woo Cho and Jong Seung Lee at Yonsei University for providing human neural stem cells.

■ REFERENCES

(1) Reguera, G.; McCarthy, K. D.; Mehta, T.; Nicoll, J. S.; Tuominen, M. T.; Lovley, D. R. Extracellular Electron Transfer via Microbial Nanowires. *Nature* **2005**, *435*, 1098−1101.

(2) Park, I. Y.; Li, Z. Y.; Li, X. M.; Pisano, A. P.; Williams, R. S. Towards the Silicon Nanowire-Based Sensor for Intracellular Biochemical Detection. *Biosens. Bioelectron.* **2007**, *22*, 2065−2070.

(3) Al-Hilli, S. M.; Willander, M.; Ost, A.; Stralfors, P. Zno Nanorods as an Intracellular Sensor for Ph Measurements. *J. Appl. Phys.* **2007**, *102*, 084304.

(4) Shalek, A. K.; Robinson, J. T.; Karp, E. S.; Lee, J. S.; Ahn, D. R.; Yoon, M. H.; Sutton, A.; Jorgolli, M.; Gertner, R. S.; Gujral, T. S.; MacBeath, G.; Yang, E. G.; Park, H. Vertical Silicon Nanowires as a Universal Platform for Delivering Biomolecules into Living Cells. *Proc. Natl. Acad. Sci. U. S. A.* **2010**, *107*, 1870−1875.

(5) Robinson, J. T.; Jorgolli, M.; Shalek, A. K.; Yoon, M. H.; Gertner, R. S.; Park, H. Vertical Nanowire Electrode Arrays as a Scalable Platform for Intracellular Interfacing to Neuronal Circuits. *Nat. Nanotechnol.* **2012**, *7*, 180−184.

(6) Berthing, T.; Bonde, S.; Rostgaard, K. R.; Madsen, M. H.; Sorensen, C. B.; Nygard, J.; Martinez, K. L. Cell Membrane Conformation at Vertical Nanowire Array Interface Revealed by Fluorescence Imaging. *Nanotechnology* **2012**, *23*, 415102.

(7) Yum, K.; Wang, N.; Yu, M. F. Nanoneedle: A Multifunctional Tool for Biological Studies in Living Cells. *Nanoscale* **2010**, *2*, 363−372.

(8) Mieda, S.; Amemiya, Y.; Kihara, T.; Okada, T.; Sato, T.; Fukazawa, K.; Ishihara, K.; Nakamura, N.; Miyake, J.; Nakamura, C. Mechanical Force-Based Probing of Intracellular Proteins from Living Cells Using Antibody-Immobilized Nanoneedles. *Biosens. Bioelectron.* **2012**, *31*, 323−329.

(9) Yum, K.; Yu, M. F.; Wang, N.; Xiang, Y. K. Biofunctionalized Nanoneedles for the Direct and Site-Selective Delivery of Probes into Living Cells. *Biochim. Biophys. Acta, Gen. Subj.* **2011**, *1810*, 330−338.

(10) Asif, M. H.; Ali, S. M. U.; Nur, O.; Willander, M.; Brannmark, C.; Stralfors, P.; Englund, U. H.; Elinder, F.; Danielsson, B. Functionalised Zno-Nanorod-Based Selective Electrochemical Sensor for Intracellular Glucose. *Biosens. Bioelectron.* **2010**, *25*, 2205−2211.

(11) Wei, D.; Bailey, M. J. A.; Andrew, P.; Ryhanen, T. Electrochemical Biosensors at the Nanoscale. *Lab Chip* **2009**, *9*, 2123−2131.

(12) Zheng, X. T.; Li, C. M. Single Cell Analysis at the Nanoscale. *Chem. Soc. Rev.* **2012**, *41*, 2061−2071.

(13) Nain, A. S.; Amon, C.; Sitti, M. Proximal Probes Based Nanorobotic Drawing of Polymer Micro/Nanofibers. *IEEE Trans. Nanotechnol.* **2006**, *5*, 499−510.

(14) Nain, A. S.; Wong, J. C.; Amon, C.; Sitti, M. Drawing Suspended Polymer Micro-/Nanofibers Using Glass Micropipettes. *Appl. Phys. Lett.* **2006**, *89*, 183105.

(15) Suryavanshi, A. P.; Yu, M. F. Electrochemical Fountain Pen Nanofabrication of Vertically Grown Platinum Nanowires. *Nanotechnology* **2007**, *18*, 105305.

(16) Kim, J. T.; Seol, S. K.; Pyo, J.; Lee, J. S.; Je, J. H.; Margaritondo, G. Three-Dimensional Writing of Conducting Polymer Nanowire Arrays by Meniscus-Guided Polymerization. *Adv. Mater. (Weinheim, Ger.)* **2011**, *23*, 1968−1970.

(17) Campo-Deano, L.; Clasen, C. The Slow Retraction Method (Srm) for the Determination of Ultra-Short Relaxation Times in Capillary Breakup Extensional Rheometry Experiments. *J. Non-Newtonian Fluid Mech.* **2010**, *165*, 1688−1699.

(18) Tuladhar, T. R.; Mackley, M. R. Filament Stretching Rheometry and Break-up Behaviour of Low Viscosity Polymer Solutions and Inkjet Fluids. *J. Non-Newtonian Fluid Mech.* **2008**, *148*, 97−108.

(19) Rubinstein, M.; Colby, R. H. *Polymer Physics*, 1st ed.; Oxford University Press: Oxford, 2003.

(20) Choi, C. K.; Lee, K. J.; Youn, Y. N.; Jang, E. H.; Kim, W.; Min, B. K.; Ryu, W. Spatially Discrete Thermal Drawing of Biodegradable Microneedles for Vascular Drug Delivery. *Eur. J. Pharm. Biopharm.* **2013**, *83*, 224−233.

(21) Ryu, W.; Bai, S. J.; Park, J. S.; Huang, Z. B.; Moseley, J.; Fabian, T.; Fasching, R. J.; Grossman, A. R.; Prinz, F. B. Direct Extraction of Photosynthetic Electrons from Single Algal Cells by Nanoprobing System. *Nano Lett.* **2010**, *10*, 1137−1143.

(22) Seo, Y. H.; Kim, L. H.; Kim, Y. B.; Ryu, W. Nanoprobe Arrays for Multiple Single Cell Insertion Using Heterogeneous Nanosphere Lithography (Hnsl). *Nanoscale* **2013**, *5*, 7809−7813.

(23) Schwarz, K. W.; Tersoff, J.; Kodambaka, S.; Chou, Y. C.; Ross, F. M. Geometrical Frustration in Nanowire Growth. *Phys. Rev. Lett.* **2011**, *107*, 265502.

(24) Shin, N. Filler, M. A. Controlling Silicon Nanowire Growth Direction Via Surface Chemistry. *Nano Lett.* **2012**, *12*, 2865−2870.

DOI: 10.1021/acsami.5b05254
ACS Appl. Mater. Interfaces 2015, 7, 16873−16880